

000
001
002
003
004 **Learning Proximal Operators for Image Restoration** 054
005 **- Supplementary Material -** 055
006
007
008
009
010
011 Anonymous CVPR submission 056
012
013
014
015 **Contents** 057
016 **1. Derivation of analytic gradients** 058
017
018 **2. Results** 059
019 2.1. Analysis of model generality 060
020 2.2. Non-blind image deconvolution results on the benchmark dataset of Levin et al. [5] 061
021 2.3. Additional comparisons on the dataset of Schuler et al. [6] 062
022
023 **3. Errata** 063
024
025
026
027
028
029
030
031
032
033
034
035
036
037
038
039
040
041
042
043
044
045
046
047
048
049
050
051
052
053

108

1. Derivation of analytic gradients

162

109

In this section we give the derivation for the computation of several analytic gradients that are required for training. The code for both training and testing will be made publicly available together with the paper.

163

110

164

165

166

167

168

169

170

171

172

For both denoising and deconvolution tasks, the \mathbf{x}^t -update in Eq. 1 has a closed-form solution, which is given in Eq. 8 and 9 in the main paper. In this supplemental document we present a derivation with the more general formula $\mathbf{x}^t = \boldsymbol{\Pi}_t^{-1} \boldsymbol{\Lambda}_t$.

172

173

In our method, the trainable parameters $\Omega = \{\lambda_p, \Theta\}$ include the fidelity weight λ_p for each problem class p , and the model parameters Θ of the proximal fields that are shared across all problem classes. The training loss function ℓ is defined as the negative of the average Peak Signal-to-Noise Ratio (PSNR) between the reconstructed and ground truth images. The gradient of the loss ℓ w.r.t. Θ is computed by averaging the gradients of all images, while the gradient of the loss ℓ w.r.t. λ_p is computed by averaging the gradients of only those images that belong to class p . For convenience, we give the derivations for one image, and omit the class label p below.

173

174

174

175

176

177

178

179

$$\ell = -20 \log_{10} \left(\frac{255\sqrt{M}}{\|\mathbf{x}^T - \mathbf{x}_{\text{true}}\|_2} \right), \quad (2)$$

180

where M is the number of pixels in each image, \mathbf{x}_{true} is the ground truth image, and \mathbf{x}^T is the reconstructed image.

181

182

182

$$\frac{\partial \ell}{\partial \Omega} = \sum_{t=1}^T \left(\frac{\partial \mathbf{x}^t}{\partial \lambda} \frac{\partial \ell}{\partial \mathbf{x}^t} + \frac{\partial \mathbf{z}^t}{\partial \Theta} \left(\frac{\partial \ell}{\partial \mathbf{z}^t} + \frac{\partial \mathbf{x}^t}{\partial \mathbf{z}^t} \frac{\partial \ell}{\partial \mathbf{x}^t} \right) \right) = \sum_{t=1}^T \left(\frac{\partial \mathbf{x}^t}{\partial \lambda} + \frac{\partial \mathbf{z}^t}{\partial \Theta} \frac{\partial \mathbf{x}^t}{\partial \mathbf{z}^t} \right) \frac{\partial \ell}{\partial \mathbf{x}^t} \quad (3)$$

183

whereby we used $\partial \ell / \partial \mathbf{z}^t = 0$. Next, we provide the derivation for the partial derivative terms in Eq. 3:

184

$$\frac{\partial \mathbf{x}^t}{\partial \lambda} = \frac{\partial \boldsymbol{\Lambda}_t}{\partial \lambda} \boldsymbol{\Pi}_t^{-1} - (\boldsymbol{\Pi}_t^{-1} \boldsymbol{\Lambda}_t)^T \frac{\partial \boldsymbol{\Pi}_t}{\partial \lambda} \boldsymbol{\Pi}_t^{-1} = \left(\frac{\partial \boldsymbol{\Lambda}_t}{\partial \lambda} - \frac{\partial \boldsymbol{\Pi}_t \mathbf{x}^t}{\partial \lambda} \right) \boldsymbol{\Pi}_t^{-1} = (\mathbf{A}^T \mathbf{b} - \mathbf{A}^T \mathbf{A} \mathbf{x}^t)^T \boldsymbol{\Pi}_t^{-1} \quad (4)$$

185

186

186

187

$$\frac{\partial \mathbf{x}^t}{\partial \mathbf{z}^t} = \frac{\partial \boldsymbol{\Lambda}_t}{\partial \mathbf{z}^t} \boldsymbol{\Pi}_t^{-1} - (\boldsymbol{\Pi}_t^{-1} \boldsymbol{\Lambda}_t)^T \frac{\partial \boldsymbol{\Pi}_t}{\partial \mathbf{z}^t} \boldsymbol{\Pi}_t^{-1} = \frac{\partial \boldsymbol{\Lambda}_t}{\partial \mathbf{z}^t} \boldsymbol{\Pi}_t^{-1} = \rho^t \boldsymbol{\Pi}_t^{-1} \quad (5)$$

188

189

189

$$\frac{\partial \ell}{\partial \mathbf{x}^{t-1}} = \frac{\partial \mathbf{x}^t}{\partial \mathbf{x}^{t-1}} \frac{\partial \ell}{\partial \mathbf{x}^t} = \frac{\partial \mathbf{z}^t}{\partial \mathbf{x}^{t-1}} \frac{\partial \mathbf{x}^t}{\partial \mathbf{z}^t} \frac{\partial \ell}{\partial \mathbf{x}^t} = \rho^t \frac{\partial \mathbf{z}^t}{\partial \mathbf{x}^{t-1}} \boldsymbol{\Pi}_t^{-1} \frac{\partial \ell}{\partial \mathbf{x}^t} \quad (6)$$

190

191

191

192

To compute the gradient of \mathbf{z}^t w.r.t. \mathbf{x}^{t-1} and Θ , i.e. $\partial \mathbf{z}^t / \partial \mathbf{x}^{t-1}$ and $\partial \mathbf{z}^t / \partial \Theta$, let's first recall Eq. 6 in the main paper:

193

$$\mathbf{z}_k^t = \mathbf{z}_{k-1}^t - \sum_{i=1}^N \mathbf{F}_i^k \psi_i^k(\mathbf{F}_i^k \mathbf{z}_{k-1}^t), \quad s.t. \quad \mathbf{z}_0^t = \mathbf{x}^{t-1}, \quad k = 1, 2, \dots, K. \quad (7)$$

194

195

195

Note that \mathbf{x}^{t-1} only appears at the first stage $k = 1$:

196

$$\mathbf{z}_1^t = \mathbf{z}_0^t - \sum_{i=1}^N \mathbf{F}_i^1 \psi_i^1(\mathbf{F}_i^1 \mathbf{z}_0^t) = \mathbf{x}^{t-1} - \sum_{i=1}^N \mathbf{F}_i^1 \psi_i^1(\mathbf{F}_i^1 \mathbf{x}^{t-1}) \quad (8)$$

197

198

200

$$\frac{\partial \mathbf{z}^t}{\partial \mathbf{x}^{t-1}} = \frac{\partial \mathbf{z}_K^t}{\partial \mathbf{x}^{t-1}} = \frac{\partial \mathbf{z}_1^t}{\partial \mathbf{x}^{t-1}} \frac{\partial \mathbf{z}_K^t}{\partial \mathbf{z}_1^t} = \left(\mathbf{I} - \sum_{i=1}^N \mathbf{F}_i^1 \psi_i'^1(\mathbf{F}_i^1 \mathbf{x}^{t-1}) \mathbf{F}_i^1 \right) \frac{\partial \mathbf{z}_K^t}{\partial \mathbf{z}_1^t}, \quad (9)$$

201

202

202

where \mathbf{I} is an identity matrix, and $\partial \mathbf{z}_K^t / \partial \mathbf{z}_1^t$ can be computed by following the rule below:

203

$$\frac{\partial \mathbf{z}_k^t}{\partial \mathbf{z}_{k-1}^t} = \mathbf{I} - \sum_{i=1}^N \mathbf{F}_i^k \psi_i''^k(\mathbf{F}_i^k \mathbf{z}_{k-1}^t) \mathbf{F}_i^k, \quad k = 1, 2, \dots, K \quad (10)$$

204

205

205

206

207

208

209

210

211

212

213

214

215

216 $\partial \mathbf{z}^t / \partial \Theta$ in Eq. 3 is composed of $\partial \mathbf{z}^t / \partial \mathbf{f}_i^k$ and $\partial \mathbf{z}^t / \partial \psi_i^k$, which are computed as follows: 270
 217

$$218 \quad \frac{\partial \mathbf{z}^t}{\partial \mathbf{f}_i^k} = \frac{\partial \mathbf{z}_k^t}{\partial \mathbf{f}_i^k} \frac{\partial \mathbf{z}_K^t}{\partial \mathbf{z}_k^t} = - \frac{\partial \mathbf{F}_i^{k^\top} \psi_i^k (\mathbf{F}_i^k \mathbf{z}_{k-1}^t)}{\partial \mathbf{f}_i^k} \frac{\partial \mathbf{z}_K^t}{\partial \mathbf{z}_k^t} \quad (11) \\ 219 \quad 272 \\ 220 \quad 273 \\ 221 \quad 274$$

$$222 \quad \frac{\partial \mathbf{z}^t}{\partial \psi_i^k} = \frac{\partial \mathbf{z}_k^t}{\partial \psi_i^k} \frac{\partial \mathbf{z}_K^t}{\partial \mathbf{z}_k^t} = - \frac{\partial \mathbf{F}_i^{k^\top} \psi_i^k (\mathbf{F}_i^k \mathbf{z}_{k-1}^t)}{\partial \psi_i^k} \frac{\partial \mathbf{z}_K^t}{\partial \mathbf{z}_k^t} \quad (12) \\ 223 \quad 276 \\ 224 \quad 277 \\ 225 \quad 278 \\ 226 \quad 279$$

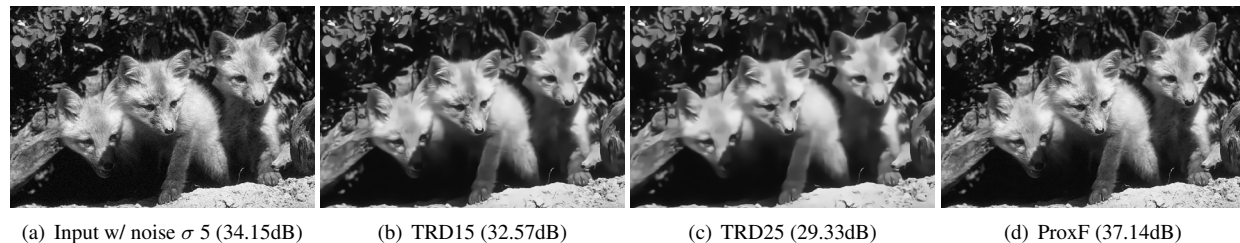
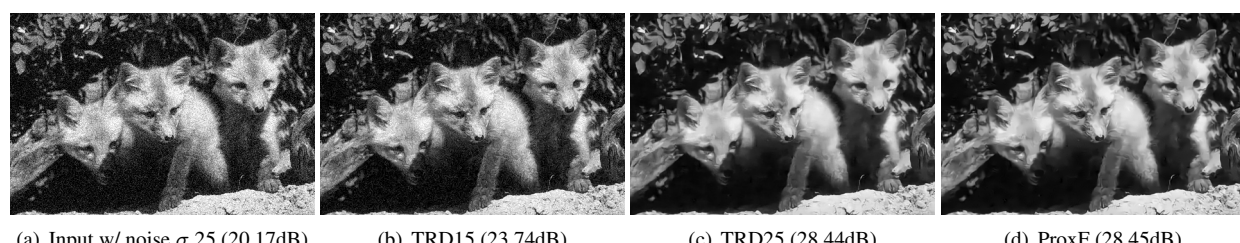
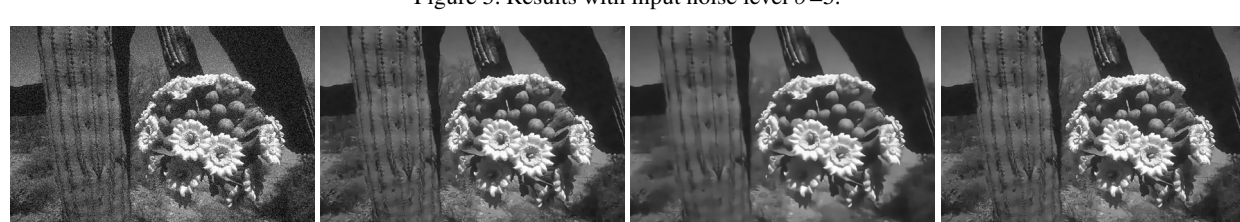
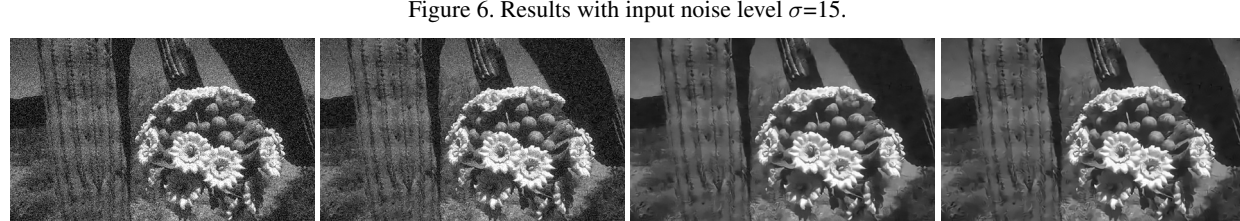
2. Results

2.1. Analysis of model generality

In Fig. 1-10, we show example images from the experiments regarding our model generality analysis that is summarized and reported in Fig. 2 in the main paper. Our method “ProxF” is trained with mixed noise levels in a single pass. The compared methods, “TRD15” and “TRD25” are trainable nonlinear reaction diffusion (TRD) models [7] that are trained at single noise levels $\sigma = 15$ and 25 respectively. Despite performing slightly below the TRD models trained for the exact noise level used at test time, our method is more generic and works robustly for various noise levels. Note that our model contains 40% fewer trainable parameters than the compared TRD models. Besides, our method uses the fidelity weight λ that is learned for each noise level at training, although adjusting its value at test time can expectedly improve our results. The learned value $\lambda = 20.706$ for $\sigma = 5$, $\lambda = 2.475$ for $\sigma = 15$, and $\lambda = 0.033$ for $\sigma = 25$. Please zoom in the figures for better view.



253 Figure 1. Ground truth images for the experiments in Fig. 2-10 307
 254 308
 255 309
 256 310
 257 311
 258 312
 259 313
 260 314
 261 315
 262 316
 263 317
 264 318
 265 319
 266 320
 267 321
 268 322
 269 323

Figure 2. Results with input noise level $\sigma=5$.Figure 3. Results with input noise level $\sigma=15$.Figure 4. Results with input noise level $\sigma=25$.Figure 5. Results with input noise level $\sigma=5$.Figure 6. Results with input noise level $\sigma=15$.Figure 7. Results with input noise level $\sigma=25$.

432
433
434
435
436
437
438
439
440
441
442
443
444
445
446
447448 (a) Input w/ noise $\sigma = 5$ (34.15dB) (b) TRD15 (33.29dB) (c) TRD25 (29.95dB) (d) ProxF (38.02dB)449 Figure 8. Results with input noise level $\sigma=5$.

450

466 (a) Input w/ noise $\sigma = 15$ (24.61dB) (b) TRD15 (32.31dB) (c) TRD25 (30.11dB) (d) ProxF (32.03dB)467 Figure 9. Results with input noise level $\sigma=15$.

468

484 (a) Input w/ noise $\sigma = 25$ (20.17dB) (b) TRD15 (23.94dB) (c) TRD25 (29.72dB) (d) ProxF (29.40dB)485 Figure 10. Results with input noise level $\sigma=25$.486
487
488
489
490
491
492
493
494
495
496
497
498
499
500
501502
503
504
505
506
507
508
509
510
511
512
513
514
515
516
517
518
519520
521
522
523
524
525
526
527
528
529
530
531
532
533
534
535
536
537538
539

540 **2.2. Non-blind image deconvolution results on the benchmark dataset of Levin et al. [5]** 594
541542 In Fig.11-18, we show our result images of the non-blind deconvolution experiments reported in Table 4 in the main paper. 595
543

Figure 11. Results on images with blur kernel #1

CVPR 2017 Submission #2043. CONFIDENTIAL REVIEW COPY. DO NOT DISTRIBUTE.

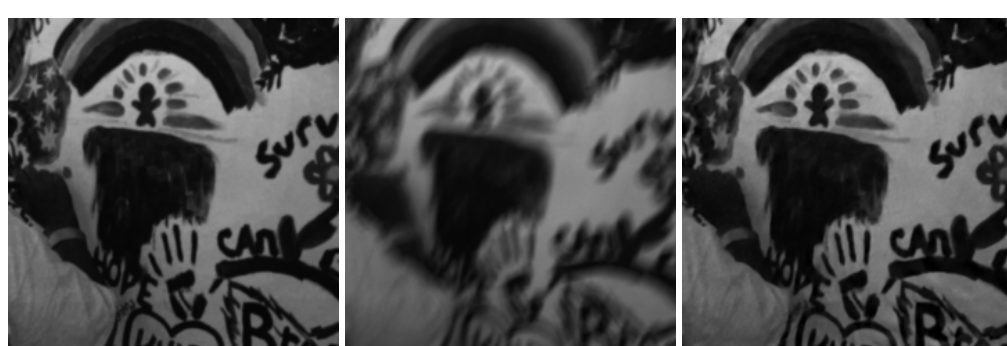
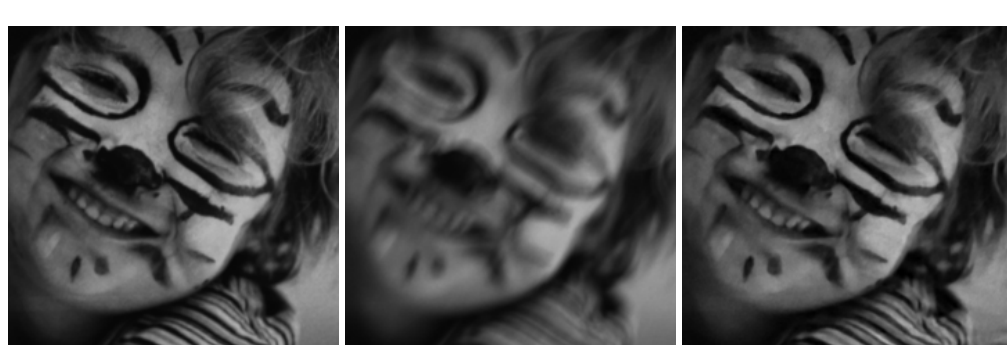
648
649
650
651
652
653
654
655
656
657
658
659
660(a) Ground truth (b) Input (22.81dB) (c) ProxF₃³ (32.36dB)661
662
663
664
665
666
667
668
669
670
671(d) Ground truth (e) Input (21.62dB) (f) ProxF₃³ (32.52dB)672
673
674
675
676
677
678
679
680
681
682
683(g) Ground truth (h) Input (22.44dB) (i) ProxF₃³ (32.90dB)686
687
688
689
690
691
692
693
694
695
696(j) Ground truth (k) Input (23.20dB) (l) ProxF₃³ (31.68dB)697
698
699
700
701702
703
704
705
706
707
708
709
710
711
712
713
714715
716
717
718
719
720
721
722
723
724
725726
727
728
729
730
731
732
733
734
735
736
737738
739
740
741
742
743
744
745
746
747
748
749
750
751
752
753
754
755

Figure 12. Results on images with blur kernel #2

CVPR 2017 Submission #2043. CONFIDENTIAL REVIEW COPY. DO NOT DISTRIBUTE.

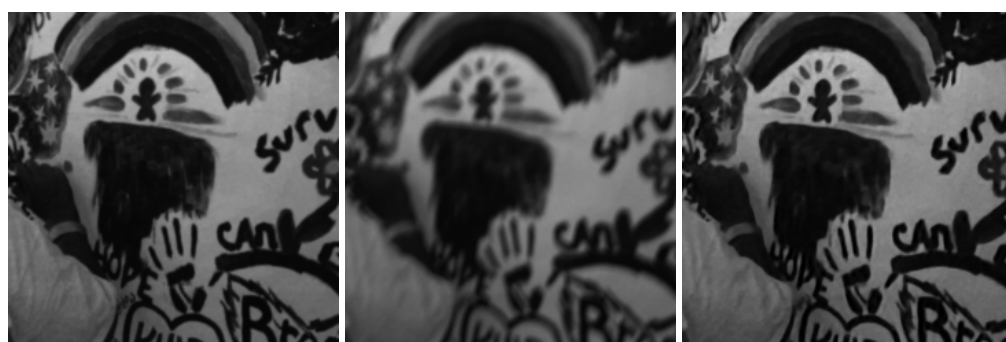
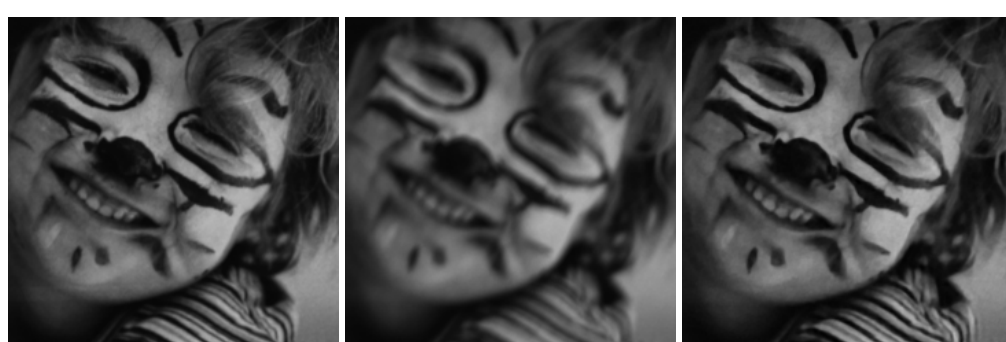
756
757
758
759
760
761
762
763
764
765
766
767
768(a) Ground truth (b) Input (26.01dB) (c) ProxF_3^3 (35.37dB)769
770
771
772
773
774
775
776
777
778
779(d) Ground truth (e) Input (24.32dB) (f) ProxF_3^3 (34.43dB)780
781
782
783
784
785
786
787
788
789
790
791(g) Ground truth (h) Input (26.31dB) (i) ProxF_3^3 (35.95dB)792
793
794
795
796
797
798
799
800
801
802
803
804(j) Ground truth (k) Input (27.51dB) (l) ProxF_3^3 (36.48dB)805
806
807
808
809810
811
812
813
814
815
816
817
818
819
820
821
822823
824
825
826
827
828
829
830
831
832
833834
835
836
837
838
839
840
841
842
843
844
845
846
847848
849
850
851
852
853
854
855
856
857
858
859
860
861
862
863

Figure 13. Results on images with blur kernel #3

CVPR 2017 Submission #2043. CONFIDENTIAL REVIEW COPY. DO NOT DISTRIBUTE.

864
865
866
867
868
869
870
871
872
873
874
875
876

(a) Ground truth



(b) Input (19.24dB)

(c) ProxF₃³ (29.63dB)877
878
879
880
881
882
883
884
885
886
887

(d) Ground truth



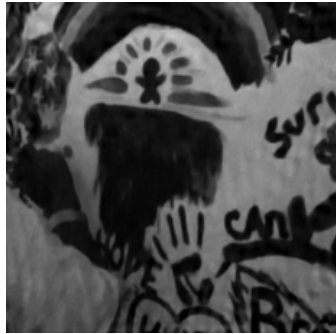
(e) Input (19.41dB)

(f) ProxF₃³ (30.68dB)888
889
890
891
892
893
894
895
896
897
898
899
900
901

(g) Ground truth



(h) Input (19.26dB)

(i) ProxF₃³ (31.63dB)902
903
904
905
906
907
908
909
910
911
912
913
914
915
916
917

(j) Ground truth



(k) Input (20.55dB)

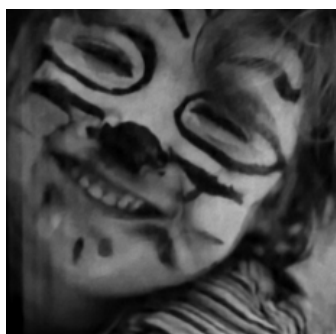
(l) ProxF₃³ (31.80dB)

Figure 14. Results on images with blur kernel #4

972
973
974
975
976
977
978
979
980
981
982
983
984

(a) Ground truth

(b) Input (26.38dB)

(c) ProxF₃³ (35.52dB)1026
1027
1028
1029
1030
1031
1032
1033
1034
1035
1036
1037
1038985
986
987
988
989
990
991
992
993
994
995

(d) Ground truth

(e) Input (25.01dB)

(f) ProxF₃³ (35.30dB)1039
1040
1041
1042
1043
1044
1045
1046
1047
1048
1049996
997
998
999
1000
1001
1002
1003
1004
1005
1006
1007
1008
1009

(g) Ground truth

(h) Input (26.39dB)

(i) ProxF₃³ (36.09dB)1050
1051
1052
1053
1054
1055
1056
1057
1058
1059
1060
1061
1062
10631010
1011
1012
1013
1014
1015
1016
1017
1018
1019
1020

(j) Ground truth

(k) Input (27.82dB)

(l) ProxF₃³ (36.38dB)1064
1065
1066
1067
1068
1069
1070
1071
1072
1073
1074
10751021
1022
1023
1024
1025

Figure 15. Results on images with blur kernel #5

CVPR 2017 Submission #2043. CONFIDENTIAL REVIEW COPY. DO NOT DISTRIBUTE.

1080
1081
1082
1083
1084
1085
1086
1087
1088
1089
1090
1091
1092

(a) Ground truth



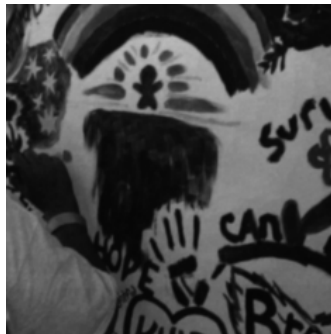
(b) Input (23.96dB)

(c) ProxF₃³ (37.68dB)1093
1094
1095
1096
1097
1098
1099
1100
1101
1102
1103

(d) Ground truth



(e) Input (22.90dB)

(f) ProxF₃³ (36.72dB)1104
1105
1106
1107
1108
1109
1110
1111
1112
1113
1114
1115

(g) Ground truth



(h) Input (23.79dB)

(i) ProxF₃³ (39.31dB)1116
1117
1118
1119
1120
1121
1122
1123
1124
1125
1126
1127
1128

(j) Ground truth



(k) Input (24.55dB)

(l) ProxF₃³ (37.79dB)1129
1130
1131
1132
11331134
1135
1136
1137
1138
1139
1140
1141
1142
1143
1144
1145
11461147
1148
1149
1150
1151
1152
1153
1154
1155
1156
11571158
1159
1160
1161
1162
1163
1164
1165
1166
1167
1168
11691170
1171
1172
1173
1174
1175
1176
1177
1178
1179
1180
1181
1182
11831184
1185
1186
1187

Figure 16. Results on images with blur kernel #6

CVPR 2017 Submission #2043. CONFIDENTIAL REVIEW COPY. DO NOT DISTRIBUTE.

1188
1189
1190
1191
1192
1193
1194
1195
1196
1197
1198
1199
1200

(a) Ground truth



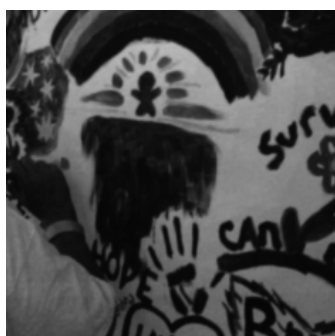
(b) Input (20.94dB)

(c) ProxF₃³ (34.47dB)1201
1202
1203
1204
1205
1206
1207
1208
1209
1210
1211

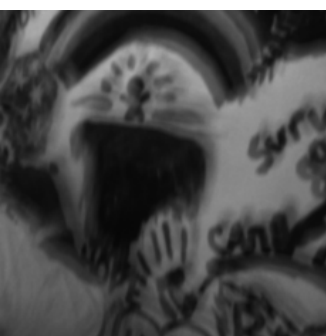
(d) Ground truth



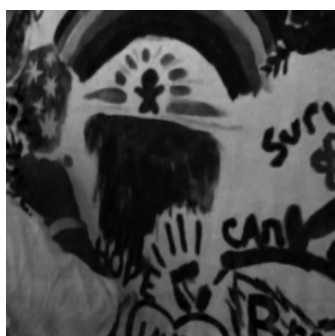
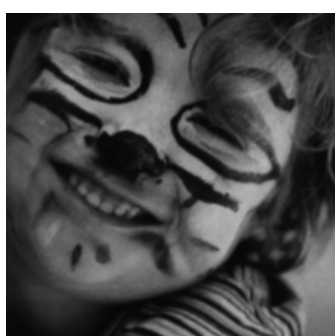
(e) Input (21.02dB)

(f) ProxF₃³ (34.23dB)1212
1213
1214
1215
1216
1217
1218
1219
1220
1221
1222
1223

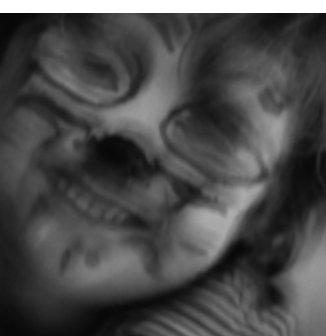
(g) Ground truth



(h) Input (21.04dB)

(i) ProxF₃³ (36.35dB)1224
1225
1226
1227
1228
1229
1230
1231
1232
1233
1234
1235
1236
1237
1238
1239
1240
1241

(j) Ground truth



(k) Input (21.83dB)

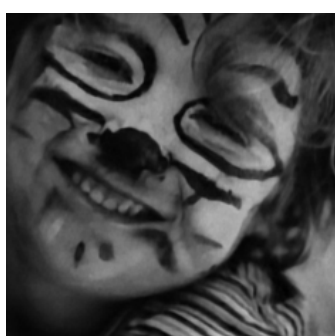
(l) ProxF₃³ (36.71dB)1242
1243
1244
1245
1246
1247
1248
1249
1250
1251
1252
1253
1254
1255
1256
1257
1258
1259
1260
1261
1262
1263
1264
1265
1266
1267
1268
1269
1270
1271
1272
1273
1274
1275
1276
1277
1278
1279
1280
1281
1282
1283
1284
1285
1286
1287
1288
1289
1290
1291
1292
1293
1294
1295

Figure 17. Results on images with blur kernel #7

CVPR 2017 Submission #2043. CONFIDENTIAL REVIEW COPY. DO NOT DISTRIBUTE.

1296



(a) Ground truth

1297



(b) Input (20.44dB)

1298

(c) ProxF₃³ (32.27dB)

1299

1300

1301

1302

1303

1304

1305

1306

1307

1308



(d) Ground truth

1309

1310

1311

1312

1313

1314

1315

1316

1317

1318

1319

1320

1321

1322

1323

1324

1325

1326

1327

1328

1329

1330

1331

1332

1333

1334

1335

1336

1337

1338

1339

1340

1341

1342

1343

1344

1345

1346

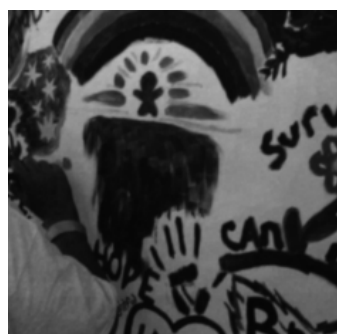
1347

1348

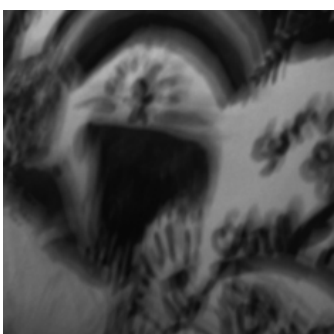
1349



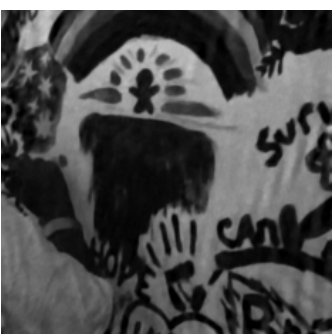
(e) Input (20.04dB)

(f) ProxF₃³ (32.36dB)

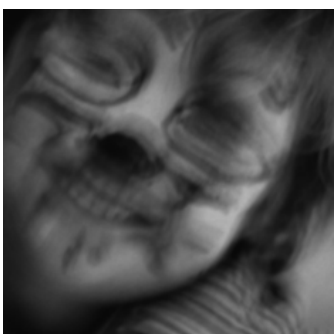
(g) Ground truth



(h) Input (20.11dB)

(i) ProxF₃³ (31.59dB)

(j) Ground truth



(k) Input (21.19dB)

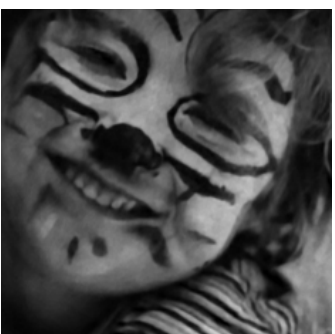
(l) ProxF₃³ (33.15dB)

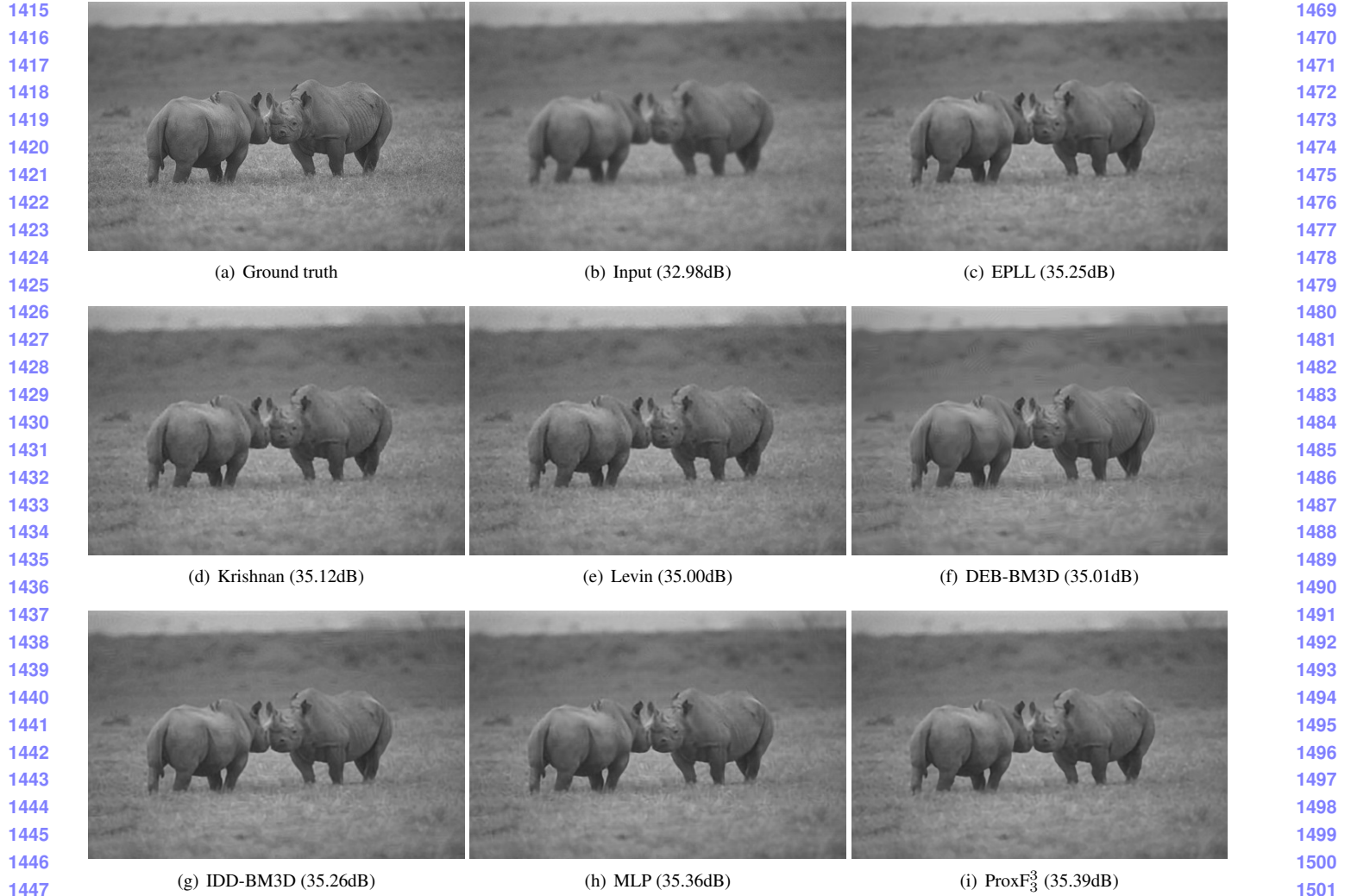
Figure 18. Results on images with blur kernel #8

1404 **2.3. Additional comparisons on the dataset of Schuler et al. [6]** 1458
1405

1406 In Fig. 19-22, we show a comparison for non-blind deconvolution on the dataset from Schuler et al. [6] that features Gaussian
 1407 blur with standard deviation 1.6 and noise level $\sigma = 2$. We compare our method ProxF₃³ with EPLL [7], Krishnan et al. [3],
 1408 Levin et al. [4], DEB-BM3D [1], IDD-BM3D [2] and MLP [6].

1409 Note that the MLP method is tailored for the task of non-blind deconvolution only and is trained with exactly the same
 1410 (single) blur kernel and noise level as those at test time [6]. In contrast, our method ProxF₃³ is trained with an ensemble of
 1411 denoising and deconvolution tasks including various blur kernels and noise levels. In particular, our training data does not
 1412 comprise any Gaussian blur kernels. Nonetheless, our method is close to MLP in terms of PSNR while at the same time
 1413 outperforming all other competitors. Please zoom in the figures for better view.

1414



1448 Figure 19. Results on non-blind deconvolution with Gaussian blur. 1502

1449

1450

1451

1452

1453

1454

1455

1456

1457

1503

1504

1505

1506

1507

1508

1509

1510

1511

1512
1513
1514
1515
1516
1517
1518
1519
1520
1521



(a) Ground truth



(b) Input (23.26dB)



(c) EPLL (25.48dB)

1523
1524
1525
1526
1527
1528
1529
1530
1531
1532



(d) Krishnan (25.56dB)



(e) Levin (25.53dB)



(f) DEB-BM3D (25.58dB)

1534
1535
1536
1537
1538
1539
1540
1541
1542
1543



(g) JDD-BM3D (25.73dB)



(h) MLP (25.93dB)



(i) ProxF₃³ (25.76dB)

1548
1548
1547
1548
1549
1550
1551
1552
1553
1554
1555
1556
1557
1558
1559
1560
1561
1562
1563
1564
1565

Figure 20. Results on non-blind deconvolution with Gaussian blur.

1620
1621
1622
1623
1624
1625
1626
1627
1628
1629

(a) Ground truth



(b) Input (24.57dB)



(c) EPLL (26.63dB)

1630
1631
1632
1633
1634
1635
1636
1637
1638
1639
1640

(d) Krishnan (26.70dB)



(e) Levin (26.69dB)



(f) DEB-BM3D (26.73dB)

1641
1642
1643
1644
1645
1646
1647
1648
1649
1650
1651

(g) IDD-BM3D (26.82dB)



(h) MLP (27.00dB)



(i) ProxF3^3 (26.85dB)

1652
1653
1654
1655
1656
1657
1658
1659
1660
1661
1662
1663
1664
1665
1666
1667
1668
1669
1670
1671
1672
1673

Figure 21. Results on non-blind deconvolution with Gaussian blur.

1674
1675
1676
1677
1678
1679
1680
1681
1682
1683
1684
1685
1686
1687
1688
1689
1690
1691
1692
1693
1694
1695
1696
1697
1698
1699
1700
1701
1702
1703
1704
1705
1706
1707
1708
1709
1710
1711
1712
1713
1714
1715
1716
1717
1718
1719
1720
1721
1722
1723
1724
1725
1726
1727

1728
1729
1730
1731
1732
1733
1734
1735
1736
1737

(a) Ground truth



(b) Input (23.54dB)



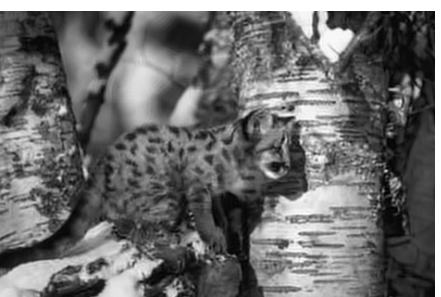
(c) EPLL (26.52dB)

1738
1739
1740
1741
1742
1743
1744
1745
1746
1747
1748

(d) Krishnan (26.53dB)



(e) Levin (26.53dB)



(f) DEB-BM3D (26.62dB)

1749
1750
1751
1752
1753
1754
1755
1756
1757
1758
1759

(g) IDD-BM3D (26.73dB)



(h) MLP (26.92dB)

(i) ProxF₃³ (26.75dB)1760
1761
1762
1763
1764
1765
1766
1767
1768
1769
1770
1771
1772
1773
1774
1775
1776
1777
1778
1779
1780
17811782
1783
1784
1785
1786
1787
1788
1789
1790
17911792
1793
1794
1795
1796
1797
1798
1799
1800
1801
18021803
1804
1805
1806
1807
1808
1809
1810
1811
1812
18131814
1815
1816
1817
1818
1819
1820
1821
1822
1823
1824
1825
1826
1827
1828
1829
1830
1831
1832
1833
1834
1835

Figure 22. Results on non-blind deconvolution with Gaussian blur.

1836	3. Errata	1890
1837		1891
1838	There is a typo in the \mathbf{x}^t -update formula in Eq. 14 of our submitted main paper. The correct version is given below:	1892
1839		1893
1840	$\mathbf{x}^t = \operatorname{argmin}_{\mathbf{x}} \lambda \ \mathbf{b} - \mathbf{Ax}\ _2^2 + \rho^t \ \mathbf{z}^t - \mathbf{x}\ _2^2 + \rho_s^t \ \mathbf{v}^t - \mathbf{x}\ _2^2,$	1894
1841		1895
1842	where in the last squared term (ρ_s^t) we omitted the erroneous 1/2 printed in the submitted paper draft. This is a typo and does	1896
1843	not affect any results in the paper.	1897
1844		1898
1845		1899
1846		1900
1847		1901
1848	References	1902
1849		1903
1850	[1] K. Dabov, A. Foi, V. Katkovnik, and K. Egiazarian. Image restoration by sparse 3d transform-domain collaborative filtering. In <i>Electronic Imaging 2008</i> . 14	1904
1851		1905
1852	[2] A. Danielyan, V. Katkovnik, and K. Egiazarian. Bm3d frames and variational image deblurring. <i>IEEE Transactions on Image Processing</i> , 21(4):1715–1728, 2012. 14	1906
1853		1907
1854	[3] D. Krishnan and R. Fergus. Fast image deconvolution using hyper-laplacian priors. In <i>NIPS 2009</i> . 14	1908
1855	[4] A. Levin, R. Fergus, F. Durand, and W. T. Freeman. Deconvolution using natural image priors. <i>Massachusetts Institute of Technology, Computer Science and Artificial Intelligence Laboratory</i> , 2007. 14	1909
1856	[5] A. Levin, Y. Weiss, F. Durand, and W. T. Freeman. Understanding and evaluating blind deconvolution algorithms. In <i>CVPR 2009</i> . 1, 6	1910
1857	[6] C. J. Schuler, H. Christopher Burger, S. Harmeling, and B. Scholkopf. A machine learning approach for non-blind image deconvolution. In <i>CVPR 2013</i> . 1, 14	1911
1858		1912
1859	[7] D. Zoran and Y. Weiss. From learning models of natural image patches to whole image restoration. In <i>ICCV 2011</i> . 14	1913
1860		1914
1861		1915
1862		1916
1863		1917
1864		1918
1865		1919
1866		1920
1867		1921
1868		1922
1869		1923
1870		1924
1871		1925
1872		1926
1873		1927
1874		1928
1875		1929
1876		1930
1877		1931
1878		1932
1879		1933
1880		1934
1881		1935
1882		1936
1883		1937
1884		1938
1885		1939
1886		1940
1887		1941
1888		1942
1889		1943